Orthogonal Recognition Processes Drive the Assembly and Replication of a [2]Rotaxane

Tamara Kosikova,[†] Nurul Izzaty Hassan,[†,‡] David B. Cordes,[†] Alexandra M. Z. Slawin,[†] and Douglas Philp*,[†]

[†]School of Chemistry and EaStCHEM, University of St Andrews, North Haugh, St Andrews KY16 9ST, United Kingdom
[‡]School of Chemical Sciences and Food Technology, Faculty of Science and Technology, Universiti Kebangsaan Malaysia, 43600 Bangi, Selangor, Malaysia

Ⓢ *Supporting Information*

ABSTRACT: Within a small, interconnected reaction network, orthogonal recognition processes drive the assembly and replication of a [2]rotaxane. Rotaxane formation is governed by a central, hydrogen-bonding-mediated binding equilibrium between a macrocycle and a linear component, which associate to give a reactive pseudorotaxane. Both the pseudorotaxane and the linear component undergo irreversible, recognition-mediated 1,3-dipolar cycloaddition reactions with a stoppering maleimide group, forming rotaxane and thread, respectively. As a result of these orthogonal recognition-mediated processes, the rotaxane and thread can act as auto-catalytic templates for their own formation and also operate as cross-catalytic templates for each other. However, the interplay between the recognition and reaction processes in this reaction network results in the formation of undesirable pseudorotaxane complexes, causing thread formation to exceed rotaxane formation in the current experimental system. Nevertheless, in the absence of competitive macrocycle-binding sites, realization of a replicating network favoring formation of rotaxane is possible.
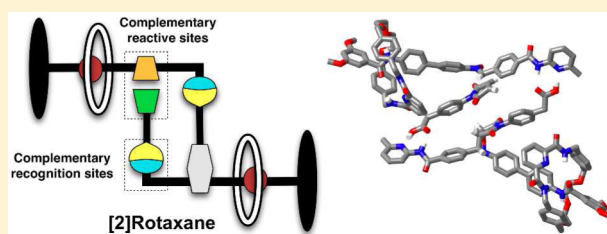
INTRODUCTION

Molecular recognition plays a pivotal role in the self-assembly[1] and self-organization[2] of both synthetic chemical systems and those found in Nature. The constitution of individual components within interconnected networks present in such systems governs their capacity to perform specific functions and to interact with other species in a recognition-mediated fashion. Small changes in the identity or orientation of recognition-enabling structural elements can have profound effects[3] on the recognition processes within a network. Therefore, careful consideration has to be given to both the desirable function-encoding elements and their relative position within a given molecular structure. Through controlled design, we can exploit the potential of molecular recognition and self-assembly as driving forces for the fabrication[4] of complex systems in a pre-organized manner. In the past, molecular recognition has been employed successfully in the formation of numerous molecular assemblies,[5] mechanically interlocked architectures,[6] nanoscale machines,[7] and systems capable of transferring structural information[8] through self-replication. Specifically, we are interested in exploring the underlying requirements that give rise to chemical systems capable of exhibiting phenomena such as self-replication. A better understanding of the principles governing assembly and replication in chemical systems will allow us to probe the requirements for molecular evolution[9] and emergence[10] of complex function. The minimal requirements for nonenzymatic, recognition-mediated replication are well understood, with a number of small-molecule examples reported[11] in the literature. However, the requirements for integrating self-replication with other recognition-mediated processes, such as those required for assembly of mechanically interlocked architectures, remain largely unexplored. Previously, we have described[12] a kinetic framework for integrating replication with the synthesis of a mechanically interlocked architecture, namely a rotaxane. However, experimental implementations of this design have not yet afforded a functional self-replicating rotaxane. Here, we propose an alternative kinetic model for the creation of a system where the assembly and replication of a [2]rotaxane is driven by two orthogonal recognition processes.

Designing a molecule capable of self-replication requires two building blocks, here termed the linear component **L** and the stoppering species **S**, equipped with complementary recognition and reactive sites. Reaction of these components (Figure 1, center) produces a template **T**. This template is capable of binding components **L** and **S** in a recognition-mediated, catalytically active ternary complex [**T·L·S**], thereby accelerating the reaction to form **T** (Figure 1, top left). Ultimately, the resulting product duplex [**T·T**] dissociates to afford two template molecules capable of taking part in further template-mediated replication cycles. Formation of a rotaxane with the capacity to replicate, however, requires an additional binding site in order to enable association between macrocyclic
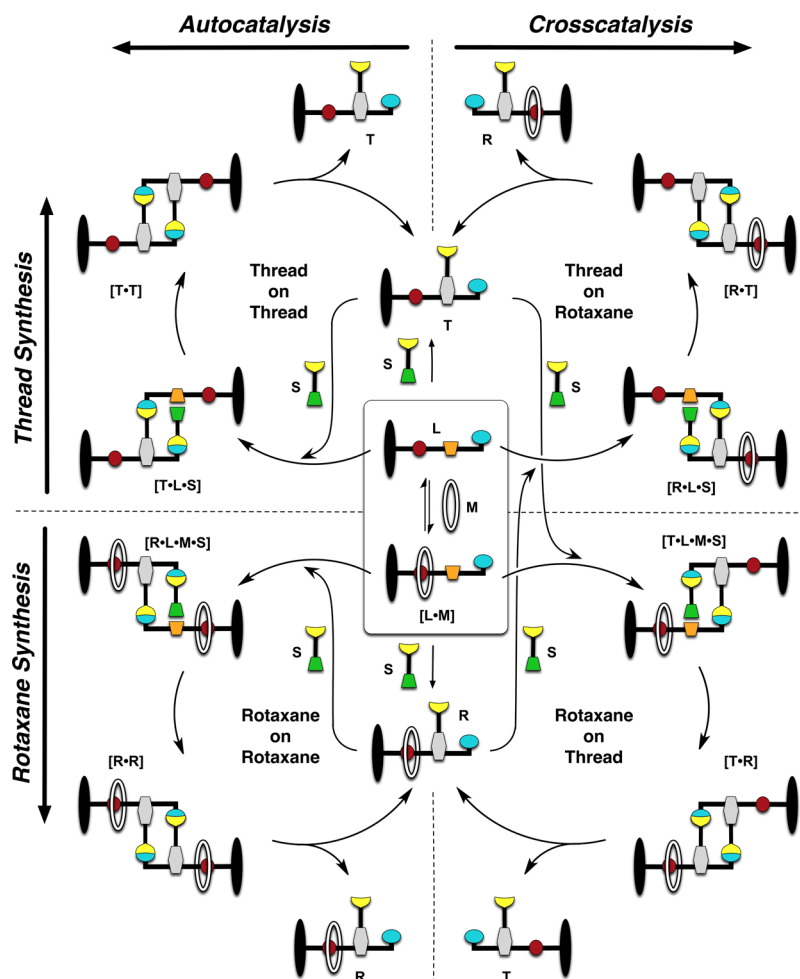
Figure 1. Kinetic model describing the main interactions in a replicating network with orthogonal recognition processes, leading to the formation of thread **T** and rotaxane **R**. The interconnected network is based around a central equilibrium (solid rectangle) between linear component **L** and macrocycle **M**, to give reactive pseudorotaxane complex [**L·M**]. The network branches out into auto-catalytic thread (top left) and rotaxane (bottom left) cycles, and cross-catalytic thread (top right) and rotaxane (bottom right) cycles. For simplicity, equilibrium arrows are not shown outside of the central equilibrium. Reactive and recognition elements are represented in cartoon form: blue and yellow represent complementary recognition sites, orange and green denote reactive elements, gray represents the reaction product, and the macrocycle-binding site is shown in dark red.

component **M** and one of the building blocks required for self-replication. In this case, the linear component **L** bears the additional macrocycle-binding site, enabling formation of a reactive pseudorotaxane complex, [**L·M**] (Figure 1, center). The replicating network radiates from this central equilibrium, established through the association of the macrocycle **M** and the linear component **L**, into separate yet interconnected thread- and rotaxane-forming catalytic cycles. Both linear component **L** and pseudorotaxane complex [**L·M**] can react with stoppering species **S** to afford thread **T** and rotaxane **R**, respectively. **T** and **R** can both establish auto-catalytic cycles, proceeding via the formation of a catalytically active ternary complex, [**T·L·S**], to make thread **T** (Figure 1, top left) and a quaternary complex, [**R·L·M·S**], to create rotaxane **R** (Figure 1, bottom left). The rotaxane and thread templates also satisfy the structural and recognition requirements necessary for taking part in cross-catalytic cycles, proceeding through [**R·L·S**] and [**T·L·M·S**] complexes (Figure 1, top right and bottom right, respectively). Overall, this interconnected replicating network can operate through two auto-catalytic and two cross-catalytic cycles. We envisaged that implementation of orthogonal

recognition processes would permit the formation of a system where all catalytic cycles are active.

Our design (Figure 2) of the key quaternary [**R·L·M·S**] complex exploits hydrogen-bonding-mediated recognition for both macrocycle binding and the complementary recognition units required for self-replication. Specifically, we exploited the recognition between a phenylacetic acid, located on the stoppering component **S**, and a 6-methyl-2-amidopyridine unit, located on linear component **L** (Figure 2a), which we have successfully employed[8d,13] in several self-replicating systems in the past. Similarly, we have utilized a 1,3-dipolar cycloaddition reaction between a nitrone, here positioned on linear component **L**, and a maleimide on stoppering element **S** as the means of irreversibly connecting the starting building blocks into a template **T** molecule (Figure 2b). From previous experience, we believed that a biphenyl spacer between the nitrone reactive site and the macrocycle binding site would be sufficient for isolating the macrocycle from the reactive site, thus preventing potential steric issues,[12] which would hinder the cycloaddition. The recognition event used to associate the macrocyclic and linear component in the pseudorotaxane complex [**L·M**] is provided by H-bonding-mediated recog-

(a)

(b)

Thread

GM [2]Rotaxane

PM [2]Rotaxane

(c)

[T·L·S]

Figure 2. (a) Cartoon representation of the chemical building blocks employed in the design of a self-replicating [2]rotaxane. The amide macrocycle-binding site (dark red) enables formation of a pseudo-rotaxane [L·M]. Amidopyridine (blue) and carboxylic acid (yellow)
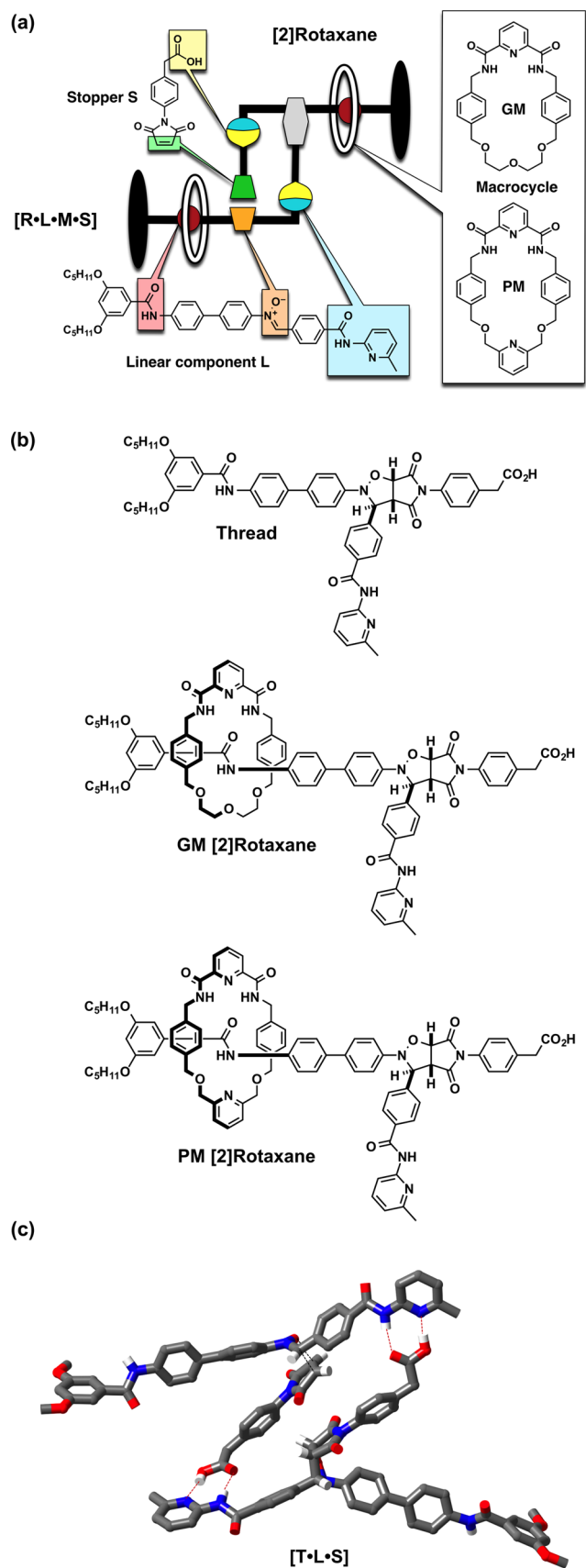
Figure 2. continued

recognition sites facilitate recognition-mediated self-replication through the formation of a quaternary complex [R·L·M·S], while the nitrone reactive site (orange) on the pseudorotaxane reacts with the maleimide (green) on the stoppering element to give the final [2]rotaxane. (b) Chemical structures of thread (**T**), **GM** [2]rotaxane (**GM-R**), and **PM** [2]rotaxane (**PM-R**). (c) Computed transition-state geometry (RM1, MOPAC 2012) for **T** being made from **L** and **S** (shown as stick representation, where carbon atoms are shown in dark gray, oxygen atoms in red, nitrogen atoms in blue, and hydrogen atoms in pale gray). Most hydrogen atoms are omitted for clarity. Red dashed lines represent hydrogen-bonds mediating the assembly of the ternary complex. Black dashed lines denote the C−O and C−C bonds partially formed in the transition state (for details, see Supporting Information).

nition between an amide group on the linear component and complementary recognition units on the macrocycle. We utilized two structurally similar macrocycles for the formation of our rotaxane (Figure 2): macrocycle **GM** employed[14] previously, containing a glycol spacer, and macrocycle **PM**,[15] incorporating a pyridine linker. Once the pseudorotaxane complex is formed, the irreversible reaction locks the macrocycle on the linear component through the stoppering approach, resulting in **GM** [2]rotaxane (**GM-R**) and **PM** [2]rotaxane (**PM-R**) (Figure 2b). Once the concentration of template present in the reaction mixture is sufficient to initiate a catalytic cycle, the reaction proceeds through the recognition-mediated replication channel (Figure 2c), with high diastereoselectivity.

■ RESULTS AND DISCUSSION

We, and others, have established[12,16] previously that various substituted diarylamides are capable of associating with macrocycle **GM**, demonstrating that the amide-containing linear component **L** is likely to be a suitable binding partner. Macrocycle **PM** contains a second pyridine ring with H-bond acceptor abilities, which we expected to bind more strongly, affording a system more selective toward the formation of a rotaxane. Initially, we performed ^{1}H NMR spectroscopic binding studies examining the association between each macrocycle and a model compound **N**, equipped with a terminal $-NO_2$ group in place of the nitrone reactive site (Figure 3). The desired amide-binding site is therefore present in isolation from any other potential recognition or reactive moieties. By reducing the temperature to 233 K, the macrocycle **N** equilibrium enters the slow exchange regime on the NMR chemical shift time scale, thus enabling direct observation of resonances corresponding to unbound species and the pseudorotaxane complex. For illustrative purposes, we will discuss only the complex formed between the compound **N** and the macrocycle **GM**. (The formation of other pseudo-rotaxane complexes is discussed in the Supporting Information.) Particularly diagnostic of pseudorotaxane formation is the downfield shift of the resonance arising from the macrocycle NH protons (Figure 3b, H^g, +1.49 ppm). The chemical shift of the macrocycle NH resonance in the bound complex (9.42 ppm) suggests that these protons are hydrogen-bonded to the carbonyl of the amide present in **N**. Macrocycle resonances arising from H^d and H^e are also shifted upfield (−0.66 and −0.56 ppm, respectively).

The inequivalence of the resonances arising from the methylene protons in the CH$_2$ group (H^a, H^b, and H^c) on
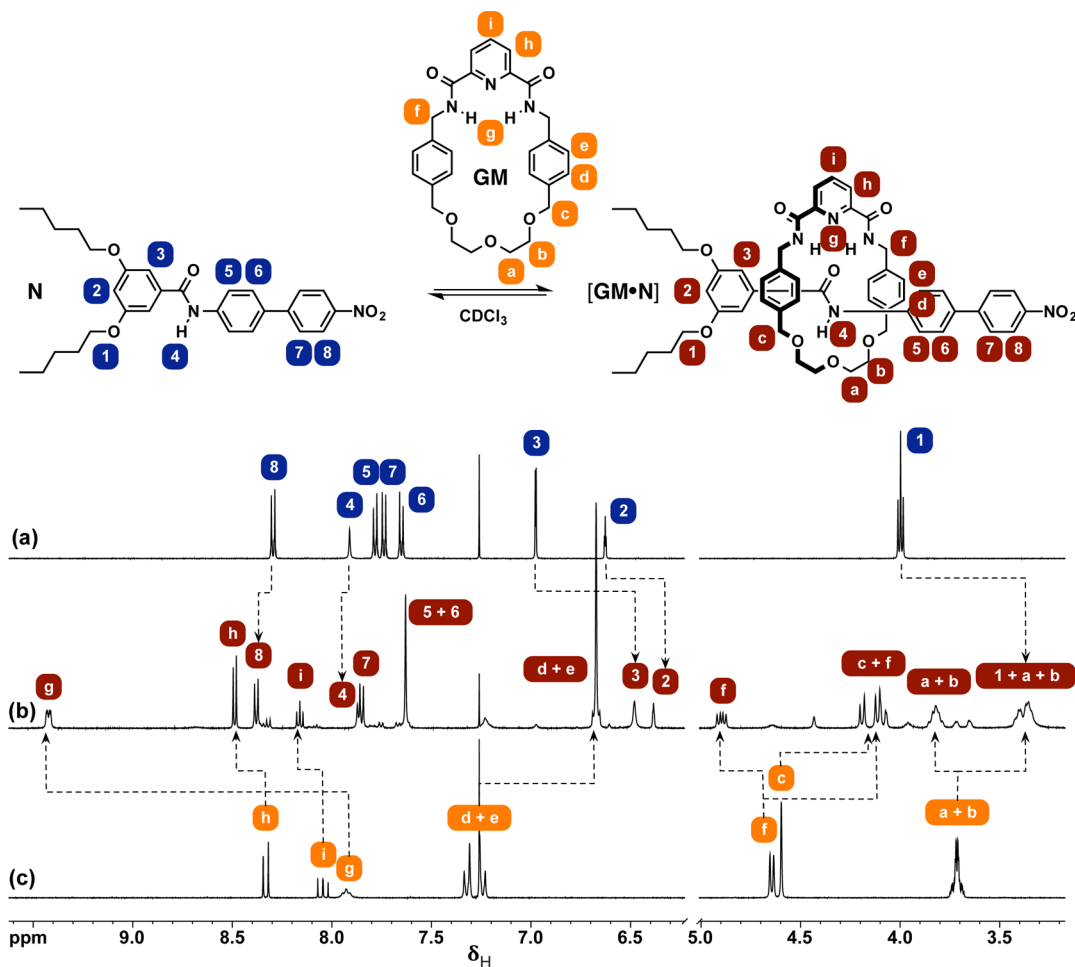
Figure 3. Partial ^{1}H NMR (500.1 MHz, CDCl$_3$) spectra of (a) compound **N** (room temperature), (b) an equimolar mixture of **N** and **GM** (233 K), and (c) **GM** (room temperature). Dashed lines are shown to connect resonances belonging to specific protons in bound and unbound states. Unassigned resonances arise from the unbound species.

the macrocycle in the pseudorotaxane is a result of the end-to-end asymmetry imposed on the macrocycle by complexation with the model compound **N**. Low-temperature ^{1}H NMR spectroscopy further allowed single-point determination of association constants with both macrocycles, affording K_a values of 3750 M^{-1} for complex [**N·GM**] and 5100 M^{-1} for complex [**N·PM**] at 223 K. For pseudorotaxane [**N·PM**], we confirmed the location of the macrocycle at the expected binding site on **N** by low-temperature (223 K) ^{1}H–^{1}H rotating-frame Overhauser effect spectroscopy (ROESY) experiments (for details, see Supporting Information), which showed ROE cross peaks between the resonances associated with the NH protons of the macrocycle and the two phenyl rings on each side of the amide present in **N**, and the resonances arising from the macrocycle CH$_2$ protons and the resonance associated with the NH of **N**. Next, we examined the association of each macrocycle with linear component **L**, which, in addition to the macrocycle-binding amide site, also contains a nitrone and an amido-pyridine, to which the macrocycles may potentially bind. The nitrone moiety in particular possesses a negatively charged oxygen atom with the potential[17] to be a hydrogen bond acceptor in the presence of complementary recognition units. The low-temperature ^{1}H–^{1}H ROESY NMR experiments, however, did not afford sharp resonances, and calculation of association constants was therefore not possible from these data. Despite these limitations, there is clear evidence for

association between **L** and **M**, suggesting that the system may be suitable for rotaxane formation.

In order to confirm successful formation of thread **T** and the two rotaxanes, **GM-R** and **PM-R**, we synthesized these products on a preparative scale by low-temperature reaction of linear component **L** and stopper **S** in the presence of excess macrocycle. All three components, **T**, **GM-R**, and **PM-R**, were isolated successfully by reverse phase flash column chromatography. Initially, we confirmed the identity of our products by matrix-assisted laser desorption/ionization time-of-flight mass spectrometry and ^{1}H and ^{13}C NMR spectroscopy. In order to further confirm that **GM-R** and **PM-R** contained the macrocycles bound at the expected site, we obtained single crystals[18] suitable for X-ray crystallographic analysis (for details, see Supporting Information). The X-ray analyses confirmed the expected molecular structures in both **GM-R** and **PM-R**, in particular the *trans* stereochemistry of the isoxazolidine ring, and the location of each macrocycle on the linear component, mediated by H-bonding interactions between the macrocycle NH and the carbonyl of the linear component (Figure 4). For both **GM-R** and **PM-R**, the crystal lattice of both rotaxanes contained a racemic mixture of the *trans* diastereoisomeric cycloadduct (Figure 4), where two molecules typically interact through H-bonding between one −COOH and one amido-pyridine recognition site, forming H-bonded chains running along the *b*-axis (**GM-R**) or *c*-axis (**PM-R**). Interestingly, the
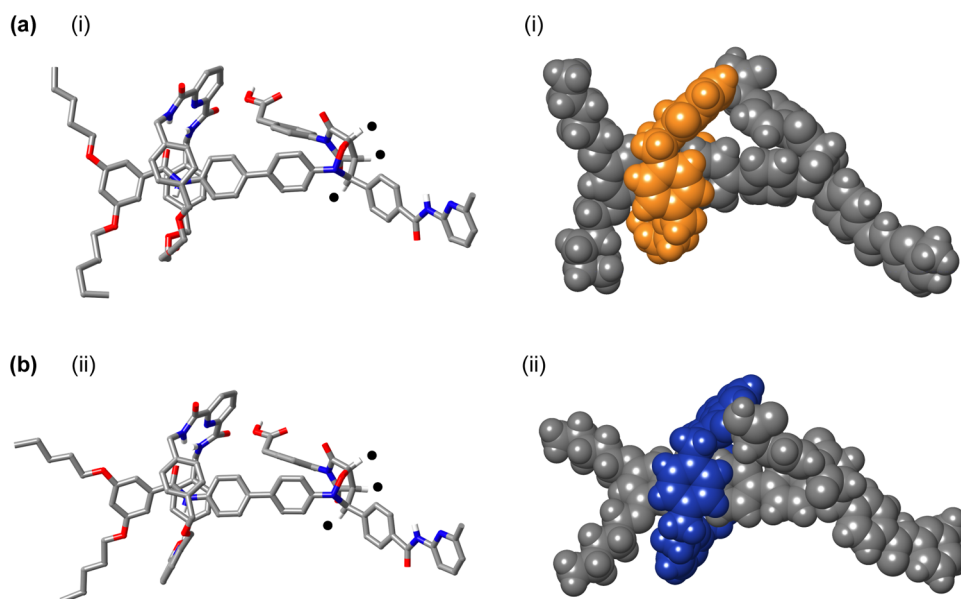
Figure 4. Stick (i) and space-filling (ii) representations of the X-ray crystal structure of (a) **GM** [2]rotaxane and (b) **PM** [2]rotaxane as determined by single-crystal X-ray crystallography. In the stick representations, carbon atoms are shown in gray, oxygen atoms in red, nitrogen atoms in blue, and hydrogen atoms in white. Most hydrogen atoms are omitted for clarity. Black circles in the rotaxane stick representations highlight the relative *trans* stereochemistry of the isoxazolidine ring protons. In the space-filling representations, the thread component is colored gray, and the macrocycle is colored either orange (**GM**) or blue (**PM**).
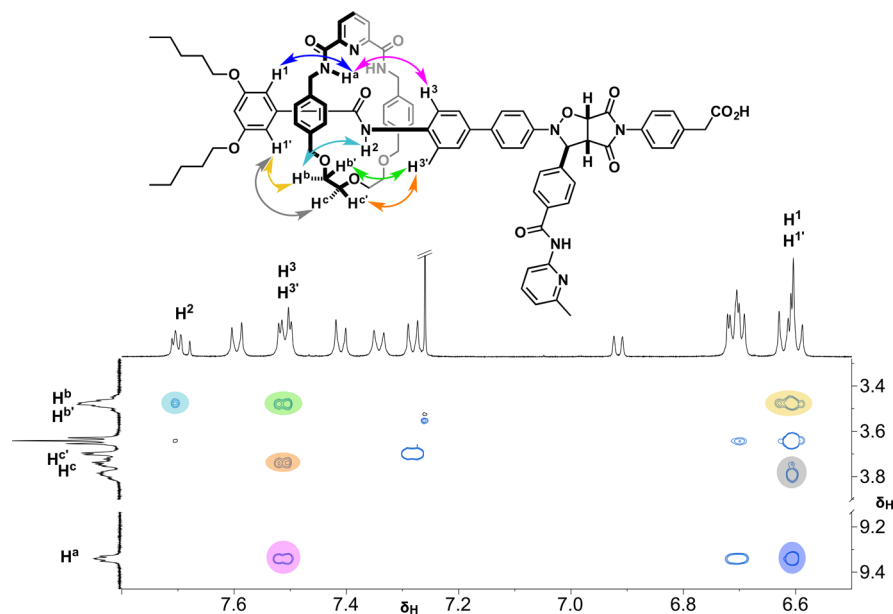

Figure 5. Partial $^1H-^1H$ ROESY correlation (500.1 MHz, CDCl$_3$, room temperature, 500 ms mixing time) of **GM** [2]rotaxane. Highlighted ROE cross peaks represent the through-space interactions between the linear component and the macrocycle. Unassigned cross peaks represent intracomponent interactions.

phenylacetic acid moiety present in the rotaxanes was directed toward the pyridine ring of each macrocycle in both **GM-R** and **PM-R**.

We conducted two-dimensional $^1H-^1H$ ROESY experiments at room temperature in order to establish the location of the macrocycle in both **GM-R** and **PM-R** on the linear component in solution. Figure 5 shows the ROE cross peaks observed in the 2D ROESY NMR spectrum of **GM-R**. Particularly diagnostic are the highlighted cross peaks associating the resonances arising from the macrocycle H^a, H^b, and H^c protons with the resonances arising from the H^1, H^2, and H^3 protons on

the linear component, confirming the expected location of **GM** macrocycle on the thread in solution. Similar results were obtained for the **PM-R** (for details, see Supporting Information).

Having synthesized and fully characterized thread **T** and both rotaxanes **GM-R** and **PM-R** successfully, we were ready to undertake a comprehensive kinetic analysis in order to ascertain which catalytic cycles (see Figure 1) are active in our rotaxane:thread system. Initially, we examined the formation of thread **T** in the absence of any added template. An equimolar mixture containing the desired components ([**L**] = [**S**] = 10
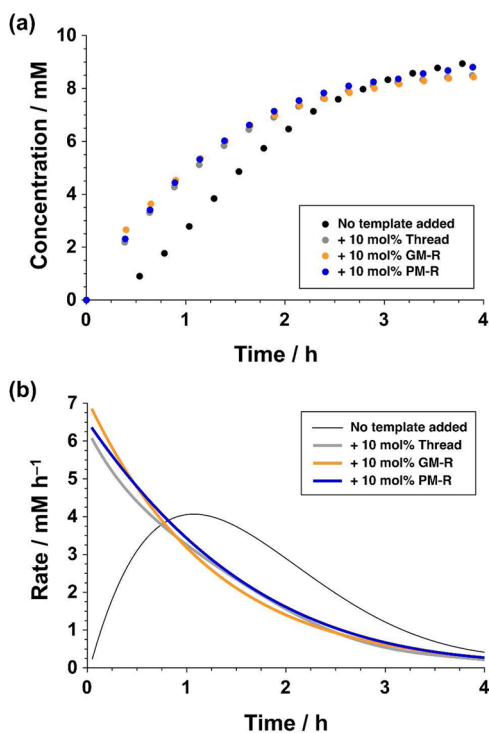
Figure 6. (a) Concentration and (b) rate profile for the formation of thread in the absence of template (black) and in the presence of pre-formed **T** (gray), 10 mol% **GM-R** (orange) or 10 mol% **PM-R** (blue) as determined by ^{1}H NMR spectroscopy (500.1 MHz, CDCl$_3$, 5 °C, all components at 10 mM). Concentration for each product was determined relative to 2,4-dinitrotoluene as an internal standard.

mM) was prepared in CDCl$_3$, and the reaction progress at 5 °C was monitored by ^{1}H NMR (500.1 MHz) spectroscopy every 15 min over 8 h. This low reaction temperature was selected for the kinetic experiments because it maximizes the strength of recognition-mediated processes within the system while simultaneously allowing accurate monitoring of the reaction progress on a reasonable time scale by ^{1}H NMR spectroscopy. The reaction time course (Figure 6a) for this reaction was determined by examining the resonances for the three protons associated with the *trans* isoxazolidine ring of the cycloadduct relative to 2,4-dinitrotoluene as an internal standard. We found that, following an initial lag period, typical for self-replicating systems, the thread replicated very efficiently, exhibiting a clear sigmoidal reaction profile where the thread concentration reached 9.1 mM after 4 h (91% conversion). We determined the rate for this reaction (d[**T**]/dt) by computing the first derivative of a seventh-order polynomial fitted to the concentration vs time data. The *trans* diastereoisomer was formed exclusively, with the rate maximum observed after 63 min (4.1 mM h^{-1}). Next, we examined the auto-catalytic formation of thread in the presence of instructing thread template. The required starting components ([**L**] = [**S**] = 10 mM) and pre-formed thread (10 mol%) were dissolved in CDCl$_3$, and the reaction progress was followed by ^{1}H NMR spectroscopy as described previously. Addition of pre-formed thread at t = 0 resulted in the disappearance of the lag period (Figure 6a), allowing the system to reach its maximum rate (6.0 mM h^{-1}) from the beginning of the reaction (Figure 6b), thereby confirming the successful design of our self-replicating system.[19] With this information in hand, we analyzed thread
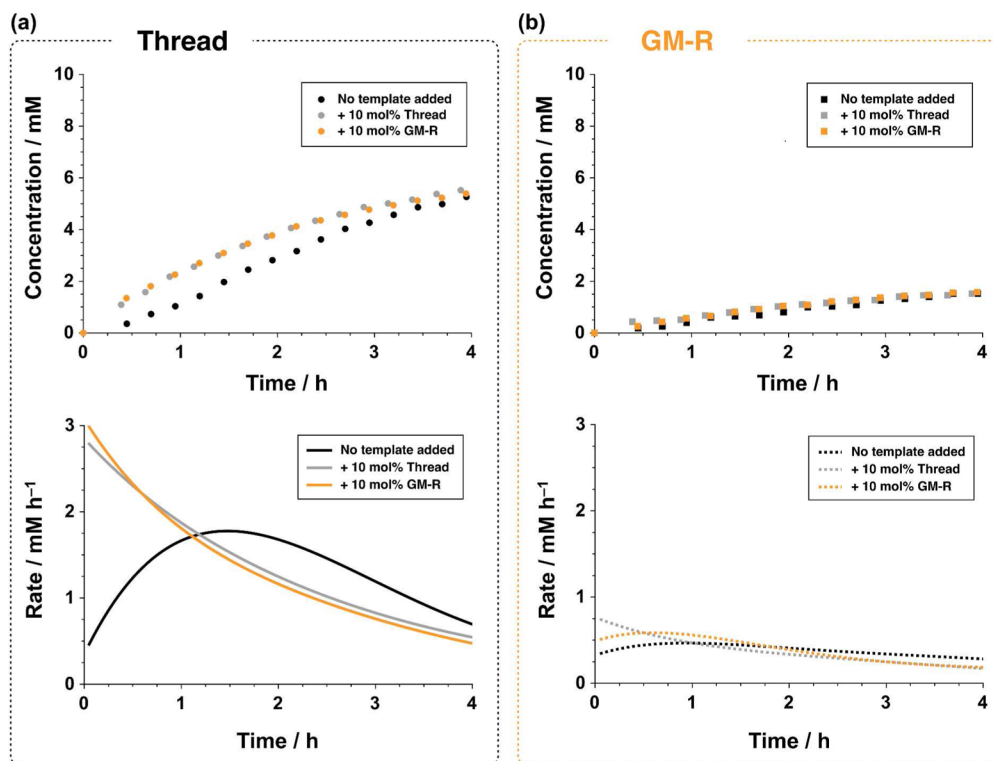

Figure 7. Concentration and rate profiles for the formation of (a) **Thread** (circles) and (b) **GM-R** (squares) in the **GM [2]rotaxane** kinetic experiments carried out in the absence of template (black) and in the presence of pre-formed 10 mol% **thread** (gray) or 10 mol% **GM-R** (orange) as determined by ^{1}H NMR spectroscopy (500.1 MHz, CDCl$_3$, 5 °C, all components at 10 mM). Concentration for each product was determined relative to 2,4-dinitrotoluene as an internal standard.

Figure 8. Concentration and rate profiles for the formation of (a) **T** (circles) and (b) **PM-R** (squares) in the **PM** [2]rotaxane kinetic experiments carried out in the absence of template (black) and in the presence of pre-formed 10 mol% **T** (gray) or 10 mol% **PM-R** (blue) as determined by ^{1}H NMR spectroscopy (500.1 MHz, CDCl$_3$, 5 °C, all components at 10 mM). Concentration for each product was determined relative to 2,4-dinitrotoluene as an internal standard.
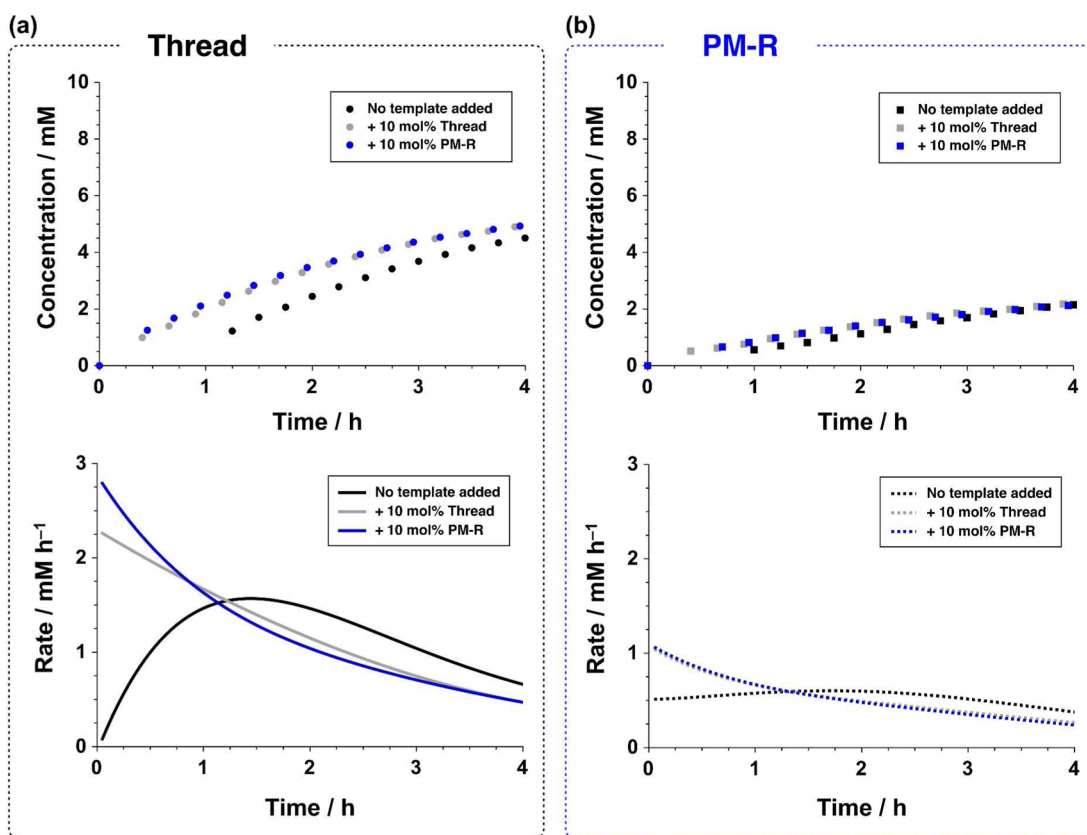
formation in the presence of 10 mol% pre-formed **GM-R** and **PM-R** (Figure 6a).

The concentration−time data for the **GM-R** and **PM-R** instructed thread kinetic experiments closely mirrored formation of thread in the presence of pre-formed thread template, showing clear disappearance of the lag period and shift in the time of maximum reaction rate (Figure 6b). The closely matching reaction profiles determined for the thread and **GM-R** and **PM-R** instructed kinetic experiments (max. rate 6.8 and 6.3 mM h^{-1}, respectively) revealed that the thread is auto-catalytic and the two rotaxanes are capable of cross-catalyzing thread formation with efficiency equal to that of thread.

Having explored the thread kinetic pathways fully, we next examined the individual, uninstructed kinetics of **GM-R** (Figure 7) and **PM-R** (Figure 8). The progress of the rotaxane kinetic experiments was again followed by ^{1}H NMR spectroscopy, allowing us to deconvolute the individual proton resonances associated with the isoxazolidine ring of each thread and rotaxane product (for details, see Supporting Information), which were formed with high diastereoselectivity for the *trans* cycloadducts.

After 4 h, **T** reached a higher concentration than either rotaxane, resulting in a 1:3 ratio of **GM-R:T** and 1:2 of **PM-R:T**, reflecting the higher affinity of the linear guest for the pyridine macrocycle **PM**. As observed in the uninstructed thread experiment, the rotaxane reaction profiles in the absence of added template revealed catalysis, exhibiting an initial lag period and sigmoidal reaction profile. In the **GM-R** kinetic

experiment, the maximum rate of product formation (Figure 7) was observed at 90 min (1.78 mM h^{-1}) for thread and 57 min (0.47 mM h^{-1}) for the rotaxane. Similarly, the maximum rate of thread formation in the **PM-R** experiment was determined at 87 min (1.57 mM h^{-1}), and at 102 min (0.60 mM h^{-1}) for the rotaxane (Figure 8).

The concentration−time profiles for the **GM-R** (Figure 7, top) and **PM-R** (Figure 8, top) rotaxane kinetic experiments in the presence of 10 mol% of pre-formed instructing thread mirrored the corresponding profiles obtained in the rotaxane kinetic experiments instructed with **GM-R** or **PM-R** template very closely, exhibiting a nearly identical ratio of **R:T** and a shortened lag period across each rotaxane set, as evidenced by the shift in the maximum rate for the formation of thread and rotaxanes to an earlier time point (Figures 7 and 8, bottom) in all instructed kinetic experiments. The outcome of the rotaxane kinetic experiments confirmed that both auto- and cross-catalytic cycles are operating in each rotaxane system with equal efficiency. Satisfyingly, results of the kinetic analyses confirmed that the orthogonal recognition processes enable formation of a replicating network where thread and rotaxane are matched in catalytic efficiencies as templates, in both auto- and cross-catalytic cycles. Nevertheless, the ratios of **R:T** determined in our kinetic experiments showed a strong preference for the formation of thread over the rotaxane in both replicating networks. This lower ratio indicates that, while the pre-formed rotaxane templates are capable of catalyzing formation of both thread and rotaxane products efficiently, the rotaxane formation itself proceeds less effectively than we had hoped based on the
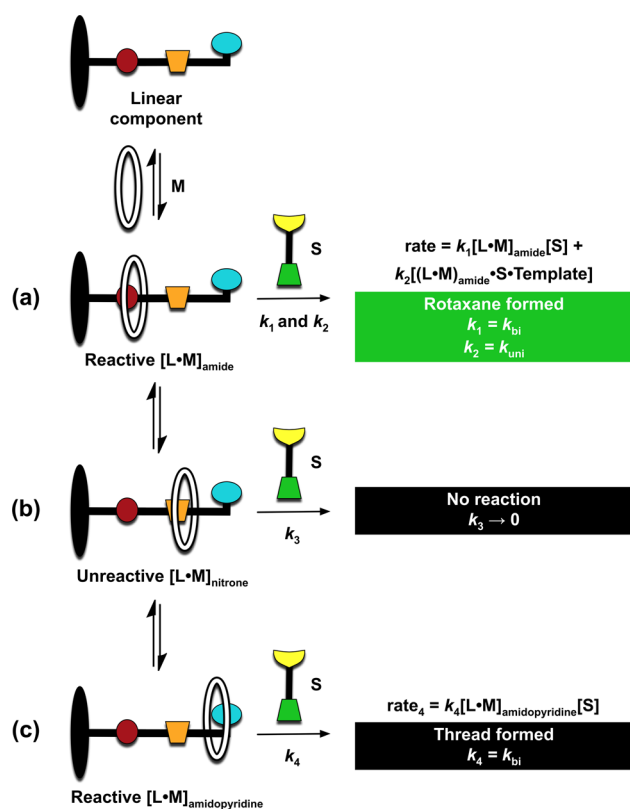
Figure 9. Model illustrating the association between macrocycle **M** and linear component **L**, affording three different pseudorotaxane complexes, only one of which results in the formation of the desired rotaxane.

Table 1. Kinetic Parameters and Association Constants Determined for the Formation of T, GM-R, and PM-R through Kinetic Simulation and Fitting of Experimental Kinetic Data (at 278 K) Using SimFit Software[a]

	T	GM-R	PM-R
k_{uni} (10^{-4} s^{1-})	226	61.0	70.4
effective molarity (M)	217	59	68
$K_a[\mathbf{L \cdot M}]$ (M^{-1})	–	220	344

[a]SimFit, by Günter von Kiedrowski, University of Bochum, 2008. In all cases, the k_{bi} and $K_{a,Duplex}$ were determined as 1.04×10^{-4} M^{-1} s^{-1} and 10.3×10^6 M^{-1} for **T**, **GM-R**, and **PM-R**.

low-temperature pseudorotaxane experiments. One plausible explanation for the low efficiency of rotaxane formation and thus the low **R:T** ratio is the insufficient proportion of each reactive pseudorotaxane complex $[\mathbf{L \cdot M}]_{amide}$ (Figure 9a), containing the macrocycle at the desired amide binding site, in each reaction as a result of the nitrone reactive site and amidopyridine recognition unit also associating with the macrocycles. The reactive pseudorotaxane complex $[\mathbf{L \cdot M}]_{amide}$ can react with stopper **S** through a bimolecular reaction ($k_1 = k_{bi}$) and, in the presence of template, also through a recognition-mediated unimolecular reaction ($k_2 = k_{uni}$). By contrast, macrocycle bound at the nitrone reactive site results in formation of a pseudorotaxane $[\mathbf{L \cdot M}]_{nitrone}$ (Figure 9b) that sequesters the **L** and **M** components in a co-conformation that hinders formation of any product. The association of the macrocycle with the amidopyridine recognition site, required for recognition-mediated self-replication, affords a pseudo-
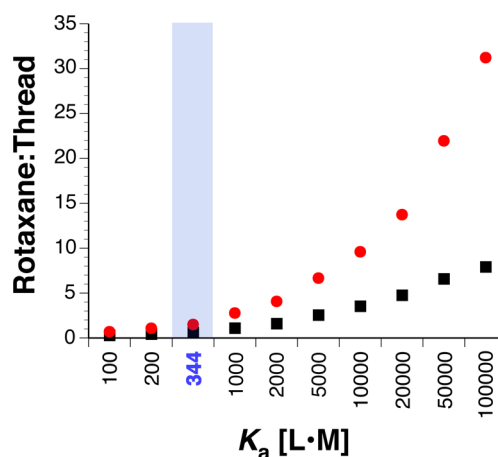

Figure 10. Outcome of kinetic simulations examining the effect of increasing K_a for the formation of pseudorotaxane complex $[\mathbf{L \cdot M}]$ on the ratio of **R:T** formed in condition A (black squares) employing kinetic parameters determined for our experimental system (k_{uni} rotaxane < k_{uni} thread) and condition B (red circles) examining an ideal system with no competitive macrocycle-binding sites on the linear component (k_{uni} rotaxane = k_{uni} thread). The blue rectangle represents the outcome of the simulation employing kinetic parameters determined for **T** and **PM-R**. Simulations were performed using SimFit software package (Günter von Kiedrowski, University of Bochum, 2008).

rotaxane complex $[\mathbf{L \cdot M}]_{amidopyridine}$ (Figure 9c) that can only react through the bimolecular pathway ($k_4 = k_{bi}$). Ultimately, the presence of these two additional sites on the linear component, capable of associating with the macrocycle, results in a smaller proportion of the desired pseudorotaxane complex $[\mathbf{L \cdot M}]_{amide}$, and, thus, a lower apparent K_a for the pseudo-rotaxane formation. The apparent K_a reflects binding of the macrocycle to three different binding sites. Similarly, the observed unimolecular rate constant (k_{uni}) associated with the template-mediated formation of each rotaxane is lower than it would be if the macrocycle were bound solely at the amide binding site.

In order to gain a better understanding of the effect of additional binding sites on this highly interconnected system, we performed fitting of all of the concentration−time data available from the related thread and rotaxane kinetic experiments to kinetic models encompassing all interactions and reactions. These models included the formation of the three different pseudorotaxane complexes in each system. Exploiting an appropriate fitting procedure (for details, see Supporting Information), we were able to extract normally inaccessible kinetic parameters, namely the template-mediated unimolecular rate constants (k_{uni}) and the product duplex association constants (K_{Duplex}) for the formation of **T**, **GM-R**, and **PM-R** (Table 1). In order to avoid fitting a larger number of constants than the data sets available, we implemented two assumptions throughout the fitting procedure: (i) k_{bi} was assumed to be identical for all three templates and (ii) only a single k_{uni} was fitted for each template across the auto- and cross-catalytic kinetic experiments forming a particular template. The latter assumption was based on the experimental observation of closely matched catalytic efficiencies determined during the kinetic experiments and the fact that attempts to fit different unimolecular rate constants for the individual auto- and cross-catalytic pathways revealed little variation in the fitted values. Interestingly, the fitting revealed that the k_{uni} values for

the formation of both rotaxanes are, as a result of the binding between each macrocycle and the linear component, almost 4 times smaller than the k_{uni} of the thread. This difference reflects a decrease in the reactivity of the rotaxane-forming, catalytically active quaternary complexes relative to the thread-forming ternary complexes. Using the fitted values of k_{bi} and k_{uni}, the effective molarity[20] for the formation of each template can be calculated. This parameter provides a measure of the efficiencies of the template-mediated catalytic pathways leading to the formation of thread and both rotaxanes, relative to the bimolecular pathways (EM = k_{uni}/k_{bi}). The apparent K_a values determined[21] for the formation of [**L·GM**] and [**L·PM**] pseudorotaxane complexes (Table 1) reflect the trend in association constants previously determined through low-temperature experiments for [**N·M**].

Analysis of the fitted kinetic parameters for thread and rotaxanes shows the detrimental effect of competitive macro-cycle-binding sites on the apparent K_a for the formation of [**L·M**] and the unimolecular rate constant and, consequently, the ratio of **R:T** formed in the system. In order to demonstrate how a similar system, integrating the formation of a rotaxane with self-replication, would work in the absence of competitive binding sites, we performed kinetic simulations. These simulations employed the parameters determined for the **PM-R** system, which exhibits more efficient rotaxane formation than **GM-R** as a result of a higher K_a for [**L·M**]. We specifically explored the effect of varying the strength of [**L·M**] association constants from 10^2 to 10^5 M^{-1} on the ratio of **R:T** ratio under two different conditions: condition A employed kinetic parameters determined for our experimental system (k_{uni} rotaxane < k_{uni} thread); condition B examined an ideal system with no competitive macrocycle-binding sites on the linear component (k_{uni} rotaxane = k_{uni} thread). Simulating condition B (Figure 10), where the effective molarity for thread and rotaxane are identical, allowed us to elucidate how the experimental system would behave in the absence of competitive binding sites—a situation where the ratio of products formed depends solely on the K_a governing the formation of [**L·M**].

The results of the simulation (Figure 10, condition A) revealed that an increase in the K_a for the association between the linear component and macrocycle does not afford an **R:T** ratio greater than 8:1 in the condition employing experimental parameters, unless K_a > 10^5 M^{-1}. While the current experimental design, incorporating two additional competing macrocycle-binding sites, does not favor rotaxane formation, the same kinetic model can afford significantly higher **R:T** ratios (>30:1) if only a single desired macrocycle binding site is present (condition B), demonstrating that rotaxane can be formed selectively in a replicating network operating simultaneously through both auto- and cross-catalytic pathways.

CONCLUSIONS

In conclusion, we have described a successful experimental implementation and full characterization of a reaction network integrating replication processes with the assembly of a [2]rotaxane. Through the application of orthogonal recognition processes, we were able to effectively direct formation of a replicating network where thread and rotaxane products are matched in catalytic efficiencies as templates, in both auto- and cross-catalytic cycles. However, interplay between the different recognition and reactive processes in the complex network, specifically the nitrone and amidopyridine moieties acting as

competitive binding sites for the macrocyclic component, resulted in thread formation surpassing rotaxane formation in the current experimental system. Exploiting kinetic simulations, we demonstrated that orthogonal recognition processes are capable of driving auto-catalytic rotaxane formation in the absence of competitive macrocycle binding sites. The realization of this goal is currently under investigation in our laboratory.

ASSOCIATED CONTENT

Ⓢ Supporting Information

The Supporting Information is available free of charge on the ACS Publications website at DOI: 10.1021/jacs.5b09738. The research data supporting this publication can be accessed at http://dx.doi.org/10.17630/d115d058-349e-4300-94e3-76a3181a9fc7.

> Experimental procedures, details of kinetic measurements, binding studies, computational modeling of the thread:rotaxane network, example fitting, and simulation scripts (PDF)
> X-ray crystallographic data for **GM-R** (CIF)
> X-ray crystallographic data for **PM-R** (CIF)

AUTHOR INFORMATION

Corresponding Author
*d.philp@st-andrews.ac.uk

Notes
The authors declare no competing financial interest.

ACKNOWLEDGMENTS

REFERENCES

(1) (a) Whitesides, G. M.; Boncheva, M. *Proc. Natl. Acad. Sci. U. S. A.* **2002**, *99*, 4769. (b) Whitesides, G. M.; Grzybowski, B. *Science* **2002**, *295*, 2418. (c) Greig, L. M.; Philp, D. *Chem. Soc. Rev.* **2001**, *30*, 287. (d) Klug, A. *Philos. Trans. R. Soc., B* **1999**, *354*, 531. (e) Philp, D.; Stoddart, J. F. *Angew. Chem., Int. Ed. Engl.* **1996**, *35*, 1154. (f) Whitesides, G. M.; Mathias, J. P.; Seto, C. T. *Science* **1991**, *254*, 1312. (g) Kushner, D. J. *Bacteriol. Rev.* **1969**, *33*, 302.

(2) (a) Lista, M.; Orentas, E.; Areephong, J.; Charbonnaz, P.; Wilson, A.; Zhao, Y.; Bolag, A.; Sforazzini, G.; Turdean, R.; Hayashi, H.; Domoto, Y.; Sobczuk, A.; Sakai, N.; Matile, S. *Org. Biomol. Chem.* **2013**, *11*, 1754. (b) Salles, A. G.; Zarra, S.; Turner, R. M.; Nitschke, J. R. *J. Am. Chem. Soc.* **2013**, *135*, 19143. (c) Northrop, B. H.; Zheng, Y.-R.; Chi, K.-W.; Stang, P. J. *Acc. Chem. Res.* **2009**, *42*, 1554. (d) Halley, J. D.; Winkler, D. A. *Complexity* **2008**, *14*, 10. (e) Karsenti, E. *Nat. Rev. Mol. Cell Biol.* **2008**, *9*, 255. (f) Epstein, I. R.; Pojman, J. A.; Steinbock, O. *Chaos* **2006**, *16*, 037101. (g) Nédélec, F. J.; Surrey, T.; Maggs, A. C.; Leibler, S. *Nature* **1997**, *389*, 305.

(3) (a) Pearson, R. J.; Kassianidis, E.; Slawin, A. M. Z.; Philp, D. *Chem. - Eur. J.* **2006**, *12*, 6829. (b) Pearson, R. J.; Kassianidis, E.; Slawin, A. M. Z.; Philp, D. *Org. Biomol. Chem.* **2004**, *2*, 3434.

(4) (a) Lehn, J.-M. *Angew. Chem., Int. Ed.* **2013**, *52*, 2836. (b) Campbell, V.; Nitschke, J. R. *Synlett* **2008**, *2008*, 3077. (c) Lehn, J.-M. *Chem. Soc. Rev.* **2007**, *36*, 151. (d) Lehn, J.-M. *Science* **2002**, *295*, 2400.

(5) (a) Chambron, J.-C.; Sauvage, J.-P. *New J. Chem.* **2013**, *37*, 49. (b) Tiefenbacher, K.; Ajami, D.; Rebek, J., Jr. *Angew. Chem., Int. Ed.* **2011**, *50*, 12003. (c) Chichak, K. S.; Cantrill, S. J.; Pease, a. R.; Chiu, S. H.; Cave, G. W. V.; Atwood, J. L.; Stoddart, J. F. *Science* **2004**, *304*, 1308. (d) Yan, H.; Park, S. H.; Finkelstein, G.; Reif, J. H.; LaBean, T.

H. *Science* **2003**, *301*, 1882. (e) Beijer, F. H.; Kooijman, H.; Spek, A. L.; Sijbesma, R. P.; Meijer, E. W. *Angew. Chem., Int. Ed.* **1998**, *37*, 75. (f) Mao, C.; Sun, W.; Seeman, N. C. *Nature* **1997**, *386*, 137. (g) Mirkin, C. A.; Letsinger, R. L.; Mucic, R. C.; Storhoff, J. J. *Nature* **1996**, *382*, 607. (h) Harada, A.; Li, J.; Kamachi, M. *Nature* **1992**, *356*, 325.

(6) (a) Gil-Ramírez, G.; Leigh, D. A.; Stephens, A. J. *Angew. Chem., Int. Ed.* **2015**, *54*, 6110. (b) Niess, F.; Duplan, V.; Diercks, C. S.; Sauvage, J.-P. *Chem. - Eur. J.* **2015**, *21*, 14393. (c) Durot, S.; Heitz, V.; Sour, A.; Sauvage, J.-P. *Top. Curr. Chem.* **2014**, *354*, 35. (d) Leigh, D. A.; Marcos, V.; Wilson, M. R. *ACS Catal.* **2014**, *4*, 4490. (e) Leigh, D. A.; Pritchard, R. G.; Stephens, A. J. *Nat. Chem.* **2014**, *6*, 978. (f) Barin, G.; Coskun, A.; Fouda, M. M. G.; Stoddart, J. F. *ChemPlusChem* **2012**, *77*, 159. (g) Beves, J. E.; Blight, B. A.; Campbell, C. J.; Leigh, D. A.; McBurney, R. T. *Angew. Chem., Int. Ed.* **2011**, *50*, 9260. (h) Stoddart, J. F. *Chem. Soc. Rev.* **2009**, *38*, 1802. (i) Haussmann, P. C.; Stoddart, J. F. *Chem. Rec.* **2009**, *9*, 136. (j) Griffiths, K. E.; Stoddart, J. F. *Pure Appl. Chem.* **2008**, *80*, 485. (k) Stoddart, J. F.; Tseng, H.-R. *Proc. Natl. Acad. Sci. U. S. A.* **2002**, *99*, 4797.

(7) (a) Kay, E. R.; Leigh, D. A. *Angew. Chem., Int. Ed.* **2015**, *54*, 10080. (b) de Bo, G.; Kuschel, S.; Leigh, D. A.; Lewandowski, B.; Papmeyer, M.; Ward, J. W. *J. Am. Chem. Soc.* **2014**, *136*, 5811. (c) Carlone, A.; Goldup, S. M.; Lebrasseur, N.; Leigh, D. A.; Wilson, A. *J. Am. Chem. Soc.* **2012**, *134*, 8321. (d) Kay, E. R.; Leigh, D. A.; Zerbetto, F. *Angew. Chem., Int. Ed.* **2007**, *46*, 72. (e) Vicario, J.; Katsonis, N.; Ramon, B. S.; Bastiaansen, C. W. M.; Broer, D. J.; Feringa, B. L. *Nature* **2006**, *440*, 163. (f) Schalley, C. A.; Beizai, K.; Vögtle, F. *Acc. Chem. Res.* **2001**, *34*, 465. (g) Raehm, L.; Kern, J.-M.; Sauvage, J.-P. *Chem. - Eur. J.* **1999**, *5*, 3310. (h) Gómez-López, M.; Preece, J. A.; Stoddart, J. F. *Nanotechnology* **1996**, *7*, 183. (i) Balzani, V.; Gomez-Lopez, M.; Stoddart, J. F. *Acc. Chem. Res.* **1998**, *31*, 405.

(8) (a) Plöger, T. A.; von Kiedrowski, G. *Org. Biomol. Chem.* **2014**, *12*, 6908. (b) Robertson, M. P.; Joyce, G. F. *Chem. Biol.* **2014**, *21*, 238. (c) Carnall, J. M. A.; Waudby, C. A.; Belenguer, A. M.; Stuart, M. C. A.; Peyralans, J. J.-P.; Otto, S. *Science* **2010**, *327*, 1502. (d) Kassianidis, E.; Philp, D. *Angew. Chem., Int. Ed.* **2006**, *45*, 6344. (e) Paul, N.; Joyce, G. F. *Proc. Natl. Acad. Sci. U. S. A.* **2002**, *99*, 12733. (f) Allen, V. C.; Philp, D.; Spencer, N. *Org. Lett.* **2001**, *3*, 777. (g) Wang, B.; Sutherland, I. O. *Chem. Commun.* **1997**, 1495. (h) Lee, D. H.; Granja, J. R.; Martinez, J. A.; Severin, K.; Ghadiri, M. R. *Nature* **1996**, *382*, 525. (i) Terfort, A.; von Kiedrowski, G. *Angew. Chem., Int. Ed. Engl.* **1992**, *31*, 654. (j) Rotello, V.; Hong, J.-I.; Rebek, J., Jr. *J. Am. Chem. Soc.* **1991**, *113*, 9422. (k) Tjivikua, T.; Ballester, P.; Rebek, J., Jr. *J. Am. Chem. Soc.* **1990**, *112*, 1249. (l) Zielinski, W. S.; Orgel, L. E. *Nature* **1987**, *327*, 346. (m) von Kiedrowski, G. *Angew. Chem., Int. Ed. Engl.* **1986**, *25*, 932.

(9) (a) Ruiz-Mirazo, K.; Briones, C.; de la Escosura, A. *Chem. Rev.* **2014**, *114*, 285. (b) Root-Bernstein, R. *Acc. Chem. Res.* **2012**, *45*, 2169. (c) Nitschke, J. R. *Nature* **2009**, *462*, 736. (d) Eschenmoser, A. *Tetrahedron* **2007**, *63*, 12821. (e) Stankiewicz, J.; Eckardt, L. H. *Angew. Chem., Int. Ed.* **2006**, *45*, 342.

(10) (a) Mahon, C. S.; Fulton, D. a. *Nat. Chem.* **2014**, *6*, 665. (b) Giuseppone, N. *Acc. Chem. Res.* **2012**, *45*, 2178. (c) Balazs, A. C.; Epstein, I. R. *Science* **2009**, *325*, 1632. (d) Pross, A. *Origins Life Evol. Biospheres* **2005**, *35*, 151. (e) Epstein, I. R.; Showalter, K. *J. Phys. Chem.* **1996**, *100*, 13132.

(11) (a) Vidonne, A.; Philp, D. *Eur. J. Org. Chem.* **2009**, *2009*, 593. (b) Patzke, V.; von Kiedrowski, G. *ARKIVOC* **2007**, *5*, 293.

(12) Vidonne, A.; Philp, D. *Tetrahedron* **2008**, *64*, 8464.

(13) Sadownik, J. W.; Philp, D. *Angew. Chem., Int. Ed.* **2008**, *47*, 9965.

(14) (a) Liu, P.; Li, W.; Liu, L.; Wang, L.; Ma, J. *J. Phys. Chem. A* **2014**, *118*, 9032. (b) Liu, L.; Liu, Y.; Liu, P.; Wu, J.; Guan, Y.; Hu, X.; Lin, C.; Yang, Y.; Sun, X.; Ma, J.; Wang, L. *Chem. Sci.* **2013**, *4*, 1701. (c) Hassan, N. I.; del Amo, V.; Calder, E.; Philp, D. *Org. Lett.* **2011**, *13*, 458. (d) Hsueh, S.-Y.; Kuo, C.-T.; Lu, T.-W.; Lai, C.-C.; Liu, Y.-H.; Hsu, H.-F.; Peng, S.-M.; Chen, C.-H.; Chiu, S.-H. *Angew. Chem., Int. Ed.* **2010**, *49*, 9170. (e) Hung, W.-C.; Wang, L.; Lai, C.-C.; Liu, Y.-H.; Peng, S.-M.; Chiu, S.-H. *Tetrahedron Lett.* **2009**, *50*, 267. (f) Huang, Y.

L.; Hung, W.-C.; Lai, C.-C.; Liu, Y.-H.; Peng, S.-M.; Chiu, S.-H. *Angew. Chem., Int. Ed.* **2007**, *46*, 6629.

(15) Ho, T.-H.; Lai, C.-C; Liu, Y.-H.; Peng, S.-M.; Chiu, S.-H. *Chem. - Eur. J.* **2014**, *20*, 4563.

(16) Jager, R.; Baumann, S.; Fischer, M.; Safarowsky, O.; Nieger, M.; Vogtle, F. *Liebigs Ann.* **1997**, *1997*, 2269.

(17) (a) D'Souza, D. M.; Leigh, D. A.; Mottier, L.; Mullen, K. M.; Paolucci, F.; Teat, S. J.; Zhang, S. *J. Am. Chem. Soc.* **2010**, *132*, 9465. (b) O'Neil, I. A.; Potter, A. J.; Southern, J. M.; Steiner, A.; Barkley, J. V. *Chem. Commun.* **1998**, 2511.

(18) Suitable single crystals were grown as colorless needles by slow evaporation of acetonitrile/CDCl₃ (**GM-R**) or as plates by slow evaporation from acetonitrile (**PM-R**). For more details, see Supporting Information.

(19) The recognition-disabled, bimolecular reactions to form thread and both rotaxanes from the linear component **L** and a *p*-methyl-substituted maleimide (**S**$_{dis}$) showed low conversion and low diastereoselectivity. For details, see Supporting Information.

(20) (a) Page, M. I.; Jencks, W. P. *Proc. Natl. Acad. Sci. U. S. A.* **1971**, *68*, 1678. (b) Page, M. I. *Chem. Soc. Rev.* **1973**, *2*, 295. (c) Kirby, A. J. *Adv. Phys. Org. Chem.* **1981**, *17*, 183.

(21) Throughout the fitting process, only a single K_a value was fitted for all three processes leading to the formation of the different pseudorotaxane complexes: $[\mathbf{L} \cdot \mathbf{M}]_{\text{amide}}$, $[\mathbf{L} \cdot \mathbf{M}]_{\text{nitrone}}$, and $[\mathbf{L} \cdot \mathbf{M}]_{\text{amidopyridine}}$. While the K_a governing the formation of each pseudorotaxane complex might be different, we were unable to deconvolute the three individual binding events. Therefore, in order to avoid using an inappropriately large number of variable parameters during fitting, only one association constant for the three binding processes was fitted (see fitting script in the Supporting Information).